Impact of variability of car-following parameters on road capacity: the simple case of Newell's model

Carlos Mario Gomez-Patino, Christine Buisson, Mehdi Keyvan-Ekbatani

Transportation Research Record
2022, Vol. XX(X) 1–15

DOI: 10.1177/ToBeAssigned
journals.sagepub.com/home/trr
SAGE

Impact of variability of car-following parameters on road capacity: the simple case of Newell's model

Carlos Mario Gómez Patiño[1], Christine Buisson[1] and Mehdi Keyvan-Ekbatani[2]

Abstract

We contribute to the vehicle-level analysis of two macroscopic features of the road traffic: capacity variability and capacity drop. In this paper, we focus only on the car-following behavior and leave the part related to lane-change maneuvers for the future research. In particular, we study a simplistic car-following model (Newell's with bounded acceleration) for a single-lane scenario. In this work, by introducing a speed limitation across a zone, a bottleneck with variable nominal capacity has been created. We use a continuous event-based numerical resolution method. Consequently, We are able to vary the three Newell's model parameters: maximal acceleration, minimal distance, reaction time. It has been shown that the variability of those car-following parameters (e.g., reaction-time, minimal-distance, and maximal-acceleration) has a strong impact on the pre-breakdown capacity variation and also on the queue discharge flow. It has been concluded that this parameters variability does impact the drop (provided that the maximal acceleration has a relatively high mean value). Various distribution shapes (uniform, truncated Gaussian, and Gamma) have been exploblack. It has been realized that this does not have any significant impact on the capacity distribution. Concerning the amplitude of the capacity distribution, we demonstrate that the reaction time is the parameter with the highest impact followed by the minimal distance. If all parameters vary with an amplitude of 30 %, we show that the capacity standard deviation, in this scenario without lane changes, is about half the experimental values reported in the literature.

Keywords

Parameters variability, Car-following models, Newell's model, Capacity, Capacity distribution.

Introduction

Most of the existing studies on macroscopic characteristics of freeway traffic flow are related to the traffic condition during congestion i.e. (i) bottleneck activation and the value of the capacity, especially the distributed nature of the capacity; (ii) capacity drop, namely the difference in capacity observed for the same location between the free flow and the upstream congested condition; and (iii) the traffic instabilities/ traffic oscillation (or stop and go (SG) waves).

Several works have shown that freeway capacity varies depending on external conditions such as traffic and geometric characteristics (*1–3*), specific traffic controls (*4–7*) and weather conditions (*8*). However, empirical observations reveal variations in capacity values from day to day in the same location with the same traffic control and similar weather (*1, 3, 9–11*).The aforementioned works suggest that these capacity variations can be due to physical differences in congestion occurrence mechanisms. Some researchers found that the observable congestion after the bottleneck activation can be generated with a lower or higher flow rate than the value accepted as the capacity. In this regard, (*10–12*) consider the traffic jam occurrence as a probabilistic event. As a result, we conclude that capacity is a distributed variable. Moreover, many studies have observed two different capacities:

- the maximal flow observed before congestion onset: Pre-Breakdown Capacity (PBC), and
- the maximal flow downstream of the queue, observed after the breakdown: Queue Discharge Flow (QDF).

The latter is always lower than the former, sometimes up to a difference of 30 % (*3, 9, 13, 14*). The difference in the value of the aforementioned capacities is called capacity drop (CD). This phenomenon was observed at fixed bottlenecks (e.g., merges, diverges, lane-drop, sags) (*1, 4, 5, 13*) or in random locations. Interestingly, in cases of random locations, It has been reported that the bottleneck occurrence is due to

[1]Gustave Eiffel University, University of Lyon, ENTPE, Licit, Lyon, France
[2]Complex Transport Systems Laboratory (CTSLAB), Department of Civil and Natural Resources Engineering, University of Canterbury, New Zealand

Corresponding author:
Christine Buisson, christine.buisson@univ-eiffel.fr

spontaneous SG waves (see for example: (14–16)). The two capacities (PBC and QDF) may independently vary even with same external conditions, as reported by many researchers (3, 11).

(3) reported a variability of 5.5% to 10.5 % of PBC for three different sites on US freeways. In a similar study, (11) indicated that the PBC standard deviation and the mean values for 15 different German freeways are 6.6 % to 13.5 % and 9.4 %, respectively. Similar results are reported in (17). The capacity distributions, the value of the drop and stop and go wave occurrence are often explained by the emergence of collective effects originated in microscopic phenomena. Based on the findings in the relevant literature, both lane changes and car-following contribute to these phenomena. However in this paper the focus is given solely to car-following behavior in case of capacity distribution and capacity drop. More specifically, we concentrate on car following variability impact on the distribution of capacity and the value of the capacity drop, considering that all vehicles obey the same model. We chose the simplest car following model: Newell's model (18), modified, according to (19) in order to include a finite acceleration. This allows us to limit the number of distributed parameters to three (i.e. maximal-acceleration, reaction-time, and minimal-distance).

The remainder of this paper is organized as follows. First, a thorough literature review is presented. This is followed by the description of the modeling framework. Then, an analysis of the influence of the distribution of the CF parameters in the exact event-based scheme is presented. The paper ends with a section devoted to discussion and conclusion.

Underlying microscopic reasons for macroscopic phenomena

Many researchers consider that the origin of capacity distribution, Capacity Drop (CD), and/or Stop and Go waves (SG) lies at the inter-vehicular interaction level, but, there is no consensus on the microscopic behavior generating these macroscopic observations. A comprehensive study of the impact of the behaviors interaction combinations is difficult due to the strong relationships of behaviors between longitudinal interactions and lane changes.

Before presenting the microscopic causes of the aforementioned macroscopic phenomena of traffic flow in congestion, we first detail the content of the literature on those observations and the way car-following (CF) and lane-changing (LC) are used to explain the capacity distribution, capacity drop, and oscillations triggering. This results in presentation of Table 1 where we classify the most relevant references in this regard. distinguishing the considered microscopic behavior and the approaches (e.g., observation, modeling-simulation, or both). Noticeably, very few papers were identified where an explanation of the capacity distribution is provided according to any of the microscopic phenomena.

Lane-changing approaches

As we can see in Table 1, some papers explain CD and SG by the impact of LCs, either by the influence of insertion into the target lane or exiting from the origin lane. For lane changer's inserting behavior, studies report that vehicles accept a short gap immediately after the insertion, then gradually relax to return to a normal spacing given by the speed-spacing relationship. That is known as the relaxation process (20–24).

Similarly, the potential followers in the target lane can "anticipate" the maneuver just before the insertion and create a long gap (courtesy spacing). The anticipation process is significantly different from the relaxation process (24). These two processes create a disturbance in the traffic stream that can be recovered gradually in time. It involves thus the acceleration process after a deceleration process which can lead to oscillations apparition (or SG waves). In this way, several studies conjecture that the LCs increase the probability of SG wave apparition (16, 25–28).

Consequently, vehicles can be confronted with the limited acceleration capability in the acceleration process and it can create a long-spacing in front of them. The studies (16, 22, 24, 28–30) explain that the CD phenomenon is due to the bounded acceleration after an insertion event into the target lane. Moreover, the exit maneuver from the origin lane leads to a longer gap that can incite the immediate follower to accelerate (16, 29).

Car-following approaches

We noticed previously that LC impacts the driving behavior by insertion and exit maneuvers. Then, the systematic LCs events on the road can be a good explanation for the observed traffic phenomena. However, we consider that longitudinal behavior plays also an important role in these observations. We focus now on different characteristics of the CF behavior, which can explain macroscopic phenomena (see Table 1):

- Random noise in acceleration caused by the drivers' lack of concentration in keeping a constant speed.
- Maximal-acceleration spread due to drivers' responses variability, which can generate long gaps due to acceleration difference (e.g. low acceleration vehicle behind high acceleration vehicle).
- Longitudinal driving instabilities due to external changes (e.g. sags, tunnels, roadside barriers, weather) leading to abrupt acceleration changes (e.g. overreaction).
- Intra-driver variability that reflects the changes in driving characteristics of the same driver adopting another behavior in different traffic conditions (e.g., an aggressive driver can become less aggressive after passing a traffic oscillation (27)).
- Inter-vehicle variability that denotes different characteristics inside the vehicles population (e.g. passenger cars and trucks, younger and older drivers).

Microscopic behavior explanation		Macroscopic characteristic of traffic flow in congestion: Capacity distribution	Capacity drop	Stop and Go
Lane-changing	Inserting		*(Oh & Yeo, 2015) (16), (Zheng et al., 2013) (24), (Coifman & Kim, 2011) (29)*, **(Leclercq et al., 2011) (30), (Duret et al., 2010) (22), (Leclercq et al., 2016) (28)**	*(Oh & Yeo, 2015) (16), (Ahn & Cassidy, 2007) (25) (Mauch & Cassidy, 2004) (26)*, (Zheng et al., 2011) (27)
	Exiting		*(Oh & Yeo, 2015) (16), (Coifman & Kim, 2011) (29)*	
Car-following	Inter-driver variability	**(Han & Ahn, 2018) (31)**, (Yang et al., 2017) (32)	**(Wong & Wong, 2002) (33)**	(Ossen & Hoogendoorn, 2007) (34), (Laval & Leclercq, 2010) (35)
	Intra-driver variability		**(Yuan et al., 2017) (14), (Calvert et al., 2018) (36), (Zhang & Kim., 2005) (37)** (Chen et al., 2014) (15)	
	Random noise in acceleration		**(Yuan et al., 2019) (38), (Xu & Laval, 2019) (39)**, (Xu & Laval, 2020) (40)	**(Treiber & Kesting, 2017) (41), (Xu & Laval, 2019) (39), (Ngoduy et al., 2019) (42)**, (Xu & Laval, 2020) (40), (Laval et al., 2014) (43)
	Acceleration spread		**(Yuan et al., 2017) (14)**	**(Treiber et al., 2007) (44)**
	Longitudinal driving instability		*(Goni Ros et al., 2013) (45)*	**(Treiber & Kesting, 2017) (41)**, (Zheng et al., 2011) (27)

Table 1. Classification of the literature associating each of the main macroscopic traffic characteristics observed in congestion and microscopic behavior. Depending on the approach of every paper, a color code is applied: *italic* text: observation-based paper; **bold** text: modeling/simulation-based paper; blue text: both.

Some papers consider the random noise in acceleration as the best approach to represent the human errors that are responsible for traffic instabilities independently of the unstable nature of CF models (*38, 41–43*) (this was also included in trains motion modeling (*46*)). They incorporate acceleration noise into CF models leading to stochastic nature. This analysis can explain the oscillations observed in absence of LCs. Paper (*41*) includes, in three different models (Intelligent Driver Model, Parsimonious CF model, and Full Velocity Difference Model), a white acceleration noise that is constant over time and between vehicles. First, the study highlights the fact that the three CF models lead to the same general findings. Authors observe that the acceleration noise systematically conducts to overestimate the speed standard deviation of vehicles and they conjecture that this instability mechanism alone is sufficient to reproduce the observations. The simulations demonstrate that the amplitude of the sub-critical fluctuations can increase strongly and thus can result in oscillations. Similarly, from the simulation findings, the study (*43*) argues that driver's error increases with roadway heterogeneity (e.g. upgrades) which can not only induce bottlenecks but also exacerbate oscillations growth. Paper (*41*) reports the same results (bottleneck activation and oscillation growth) for acceleration noise and action points (e.g. deceleration areas). Besides, the differences in vehicles characteristics (e.g. maximal-acceleration, reaction-time) can be accentuated depending on the road segment specificity. This can also, without LC, generate spontaneous oscillations. An aggressive driver behavior leads to hysteresis loops which induce the upstream propagation of oscillations (*15*). The authors of (*35*) propose a model which considers an upgrade (in a single lane without LC) to capture the mechanism that triggers periodic oscillations. With the parameters calibrated using NGSIM data (US-101 site), the simulation results explain oscillations as a consequence of driver heterogeneous reactions to deceleration waves.

From observations, the study (*27*) quantifies later the number of oscillations observed in two different sites, I-80 and US-101 of NGSIM data. The results suggest that oscillations can be instigated by different factors, the predominant trigger depending on the site characteristics. In the first location (waving area), the majority of the SG was originated from LCs. On the other one (uphill), 66 % of the SG were originated by longitudinal driving disturbances due to the limited perception of the road inhomogeneity. Similarly, paper (*45*) shows that oscillations upstream of a sag in Tokyo (Japan) are created in most cases by spontaneous instabilities in longitudinal behavior, rather than by LC impact. Based on these findings, the authors assume that capacity reduction is due to changes in CF behavior caused by the sag. Indeed, the impact on the traffic dynamics depends on the sag characteristics (e.g. the value of the slope angle in a downhill-uphill can influence the congestion apparition and also the number and amplitude of SG waves (*47*).

The acceleration error is not the only approach able to explain the traffic phenomena based on longitudinal interactions, also acceleration variability among drivers can be an explanation: for example, a long-spacing can be created between two successive vehicles if the follower's acceleration capability is lower than the leader's. In the same study (*14*), the authors consider a dynamical reaction-time extension in the acceleration process that depends on the congestion level. That means a negative relation between reaction-time value and speed value in congestion. The numerical findings explain that the intra-driver mechanism and its variation (reaction-time evolution) yields to a relation between the speed in congestion and the Queue Discharge Flow, as found in empirical observations. We note also that this paper introduces the intra-driver variability notion to explain CD amplitude, which means that vehicles change their driving features according to traffic conditions. For example, authors consider a driver's tendency to take a larger headway downstream of an oscillation (*14*, *15*). Oscillations affect the driver's behavior and this can result in a change of individual characteristics (e.g., aggressive drivers are less aggressive after passing the oscillation (*27*) and tend to adopt larger response times). Thus, the reduction in bottleneck discharge rate ensues even in absence of LCs (*14*). In this regard, paper (*15*) focuses on the mechanism of periodicity of traffic oscillations and finds that drivers' reactions to oscillations around a bottleneck have a profound impact on CD. Moreover, the amplitude of the oscillation could influence the acceleration/deceleration values (e.g. hysteresis level (*48*)) and thus the discharge rate (*16*).

With a modeling approach, (*37*) proposes a CF model dedicated to explaining CD under different driving conditions. Driver's time headway is assumed to be a function not only of distance headway but also of traffic conditions. Although their results were not validated with observations, this work sheds light on different spacing-speed relationships that vehicles could adopt according to the individual characteristics and the impact of this on the FD.

These characteristics of the vehicle-driver pairs explain the difference between vehicles population including the desired speed, acceleration/deceleration capability, reaction-time and accepted minimal-distance. In the present paper, the first step in a larger work, we consider this inter-vehicle variability as independent of traffic conditions.

Some papers mention reaction-time and minimal-distance distributions as inter-vehicle variability (*31*, *32*, *34*, *35*, *49*). From empirical trajectories, other studies (*34*, *50*) obtained different vehicles-drivers parameters for every specific model. They propose that inter-vehicle variability can be classified into two types: i) different driving styles (captured by different CF models) and; ii) different inter-vehicle characteristics (captured by distributed CF parameters of the same model). The study (*34*) focuses on the analysis of the inter-vehicle variability in CF by comparing heterogeneous and homogeneous platoons to study traffic stability via simulation. The simulation findings show that inter-vehicular heterogeneity influences asymptotic stability. It means that disturbance propagates quickly and can grow in magnitude from vehicle to vehicle. Indeed, the plots in Fig. 3 in (*34*) show that the traffic jam appears earlier and leads to higher congestion level due to the CF parameters variability.

Similarly, the inter-drivers difference of responses to the flow disturbance can reveal the mechanism of the probabilistic breakdown occurrence at bottlenecks (*32*, *50*). (*32*) conjectures that some following drivers are not affected by the unnoticed driving changes of their leaders as much as others at sags. To model this phenomenon, they estimate different CF parameters distributions and propose a microscopic simulation. The results explain that the congestion occurrence probability increases with the traffic demand. However, the estimated cumulative distribution function is not the same as the empirical curve. The authors link it to a potential relationship between a sub-part of the CF parameters.

The investigation in (*31*) proposes a stochastic traffic breakdown model for freeway merge bottlenecks to reveal the breakdown mechanisms considering various traffic parameters (e.g. desired speed, merging speed, wave speed, merge flow rate, individual vehicle-driver's characteristics). A Bayesian approach is developed to estimate the breakdown probability associated with the individual parameters. The analytical results show that the probability of traffic breakdown increases with higher values of drivers' reaction times and the standard deviation of headway distribution. In this paper, the standard deviation of reaction-time has no impact on the probability curve.

Research gaps

Based on the previous literature summary, we conclude that many authors consider that bounded acceleration after LC is responsible for the CD phenomenon. We note also that intra-driver variability (reaction-time evolution) is an important explanation of that phenomenon. However, several of those papers only focus on the Queue Discharge Flow (QDF) variability and the Pre-Breakdown Capacity (PBC) variability has been less analyzed. Moreover, the literature findings shed light on the impacts of acceleration variability on the CD phenomenon. Note that the inter-vehicle variability of reaction-time and minimal-distance in CF behavior were also mentioned as an important contribution to explain macroscopic observations. Consequently, for a complete analysis of macroscopic phenomena, we consider that a focus on the inter-vehicle variability between vehicles' behavior must be scrutinized, in particular in its impact on the macroscopic features of traffic like the PBC variability and CD amplitude.

The hypothesis of the present paper is that longitudinal interactions may well explain the macroscopic observations even in the absence of LCs. The aim of this analysis is to determine the link between the inter-vehicle variability of car-driver pairs and the macroscopic phenomena (PBC distribution and CD), explained only by the CF. A systematic exploration of the CF parameters variability (e.g. reaction-time, minimal-distance and maximal-acceleration) is the only way to explore the potential cumulative effects. We choose to explore a unique CF models: Newell's model (*18*) because of its low number of parameters (modified to include a finite acceleration, according to (*19*)). We show that the reaction-time is the most important parameter influencing the two macroscopic variables capacity variability amplitude and capacity drop.

Microscopic Modeling Framework

Model definition

As mentioned earlier, we use Newell's model (*18*) because of its simplicity and the fact that the parameters are translatable from the microscopic level to the macroscopic one. The equation below corresponds to the extended version of Newell's model presented in (*19*). In this equation the first line corresponds to the congested regime, and the second line to the free flow regime, τ^n, d^n, and a^n being respectively the reaction-time, the minimal-distance, and the maximal-acceleration.

$$\dot{x}_n(t) = \min\left[\min\left\{\frac{\Delta x^{n-1,n}(t) - d^n}{\tau^n}; v^n(t-\tau^n) + a^n \cdot \tau^n\right\}; v_f^n\right] \quad (1)$$

They are two differences between this version and the original one (*18*). First, we associate each vehicle-driver pair with its parameters, keeping them constant. This corresponds to our objectives as we focus on inter-vehicle variability, and we do not want to include intra-driver variability. Second, on the contrary to the original version where acceleration and deceleration are infinite, a maximal-acceleration parameter (a^n) permits to limit the acceleration in the free flow regime. Our motivation to include a^n and its variability is the literature findings of the capacity drop phenomenon (see Table 1). Note that the modified Newell's model does not include deceleration in its equation 1 (positive acceleration only being limited). More generally speaking, taking into account deceleration in CF model certainly modifies locally the car behaviors in the upstream limit of the congestion, but we believe that this may not have a strong impact on the global scale.

We keep identical, over all vehicles, the maximal desired speed ($v^n = v^f$) given that our study considers longitudinal circulation of vehicles in a single traffic lane. A slower vehicle in this single lane scheme could change the independence properties of the follower vehicles.

Simulation settings

We define the simulation settings in order to observe congestion onset without lane changes. Thus, we chose a one-lane stretch of road with a zone where speed is limited to a value U_l, lower than the free flow speed: U_f. U_l variation permits the exploration of different congestion levels. The entering time instants are defined according to:

- An input flow profile, which defines the demand in two periods: (i) the traffic flow increases linearly, from an initial flow value (q_0) to a maximal flow value (q_{max}); (ii) the traffic flow remains constant at q_{max}.We set the maximal input flow to correspond to the value of the theoretical congested capacity associated to the maximal value of the limited speed, for an illustration see Fig. 1 (top);
- The classical exponential distribution of inter-vehicular headways at the simulated zone entrance.

We can thus observe the transition conditions from the free flow regime to the congested flow regime and therefore identify the congestion onset.

The PBC is defined as the entering flow at the moment this triggering vehicle enters the link. The QDF is the mean downstream flow observed during the remaining period after this vehicles exits the speed limitation zone. Applying the formulas proposed by (*51*), we use the window size of $\Delta_t =$ 60 s and $\Delta_x =$ 100 m to measure density and flow rate during the time with a frequency of 20 s. Density and flow are used to construct the simulated fundamental diagrams. In this study, We don't consider the queue length as an output variable. It is indirectly linked to the PBC and can be inferred from its value. Note that for this test, we use an individual time-step numerical scheme (resolution based on individual

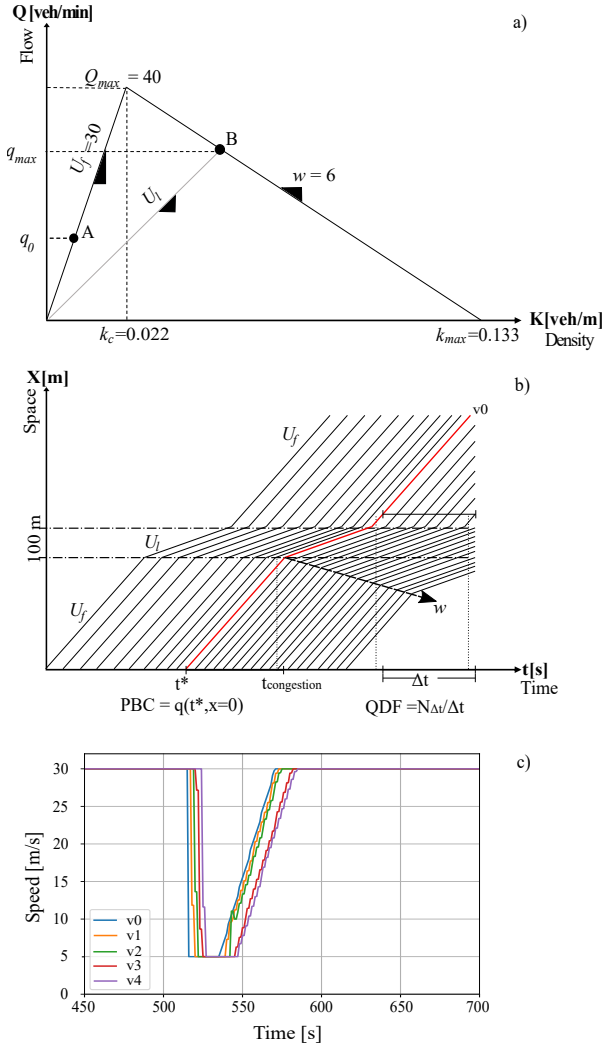

Figure 1. Description of the fundamental diagram and the capacities measurement method: a) Theoretical fundamental diagram with the physical meaning of the various macroscopic parameters with the variation range of the limited speed U_l between 5 and 20 m/s, b) measurement method of PBC and QDF, c) speed evolution of some vehicles identified immediately after the congestion onset. V_0 is the last vehicle not affected by congestion and V_1 is the triggering vehicle (represented in red in Fig. b). Congestion is considered when at least 10 vehicles are in the queue.

reaction-time value). The code is available *. Table 2 presents macroscopic and car-following parameters, as well as the various scenarios.

Distributions of car-following parameters

The simulation attributes to each driver-vehicle pair its own parameters, selected according to a distribution. We study here three different distributions:

- uniform,
- truncated Gaussian (to avoid negative values),
- gamma.

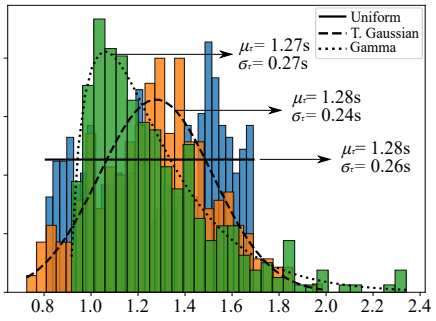

Figure 2. Parameters distributions according to the different function shape with theoretical variation amplitude of 20 %.

The uniform distribution is chosen for its simplicity, as well as the truncated Gaussian. We selected also the Gamma distribution because in the literature, some authors found this shape is adequate for the reaction-time distribution (*32*).

The Fig. 2 illustrates how the three distributions are adapted, for parameter p, to present the same (σ_p/μ_p) ratio and the same μ_p value.

For each parameter p (the reaction-time τ^n, the minimal-distance d^n and the maximal-acceleration a^n), the amplitude is defined by the ratio between the standard deviation (σ_p) value and the mean value (μ_p). We study three amplitudes for each distribution: 10 %, 20 %, 30 %.

The mean value of some parameters is directly determined from the fundamental diagram taking into account that $\mu_\tau = 1/k_{max} * w$ and $\mu_d = 1/k_{max}$. Table 2 presents the macroscopic and car-following parameters values used in the rest of the paper.

It is well known that in Newell's modeling framework, τ and d are not independent: w, the backward wave propagation speed links the two through the relation $w = d/\tau$ (*49*, *52*). Therefore, we can choose to vary d^n and τ^n independently or to vary one of them (the reaction-time τ^n, for example) and to deduce the value of d with a constant w value. This is illustrated in Fig. 3, which represents the impact on various methods of parameters random generation on the two versions of the fundamental diagrams: the macroscopic $(Q = f(K))$ and the microscopic one $(s = f'(v)$, where s is the spacing between the car and its leader, v is the speed). If w is constant (see 3.a), the capacity and the maximal density vary in the same proportion, this is not the case if d and τ vary independently.

In addition to the congestion level (defined by the limitation speed U_l), the parameter distribution function and the level of variability, each traffic scenario is characterized by the (set of) distributed parameters:

*https://github.com/carlosmgop/Variability-of-Newell-model-parameters.git

Macroscopic parameters	Description	Values	Units
U_f	free flow speed	30	m/s
w	backward wave propagation speed	6	m/s
k_{max}	maximal density	0.133	veh/m
Q_{max}	maximal capacity	40	veh/min
CF variables			
$x^n(t)$	position of vehicle n at time t		m
$\dot{x}^n(t) = v^n(t)$	speed of vehicle n at time t		m/s
$\ddot{x}^n(t)$	acceleration of vehicle n at time t		m/s^2
$\Delta x^{n-1,n}(t)$	distance of vehicle n with its leader $n-1$ at t		m
$\Delta v^{n-1,n}(t)$	speed dif. between vehicles n and $n-1$ at t		m/s
CF parameters		Mean	
τ^n	reaction-time of vehicle n	1.25	s
d^n	minimal-distance of vehicle n	7.50	m
a^n	maximal-acceleration of vehicle n	3.00	m/s^2
$v_f = U_f$	maximal desired speed (identical for all n)	30.0	m/s
Scenario definition			
U_l	speed in the speed limit zone	5 m/s, 10 m/s, 15 m/s	
	parameters distribution definition	uniform / T. Gaussian / Gamma	
	variability distribution	no / one param. / all parameters	
	variability amplitude	SD = 10 %, 20 % or 30 % of the mean	

Table 2. Macroscopic, car following variables and parameters and scenario definition of the simulation (T. Gaussian stands for "truncated Gaussian", chosen to avoid negative values)

- $\varnothing$: no variation;
- a: only the maximal-acceleration varies;
- d: only the minimal-distance varies (as a consequence, w varies), see Fig. 3.a and 3.b;
- τ: only the reaction-time varies (as a consequence, w varies), see Fig. 3.c and 3.d;
- (d, τ): in this configuration, τ and d variations are linked, w is constant; in addition, the acceleration varies, Fig. 3.e and 3.f;
- $All\ Var$: all parameters vary, independently, see Fig. 3.g and 3.h.

The simulation considers 100 replications of each traffic scenario to obtain the distributions of PBC and QDF.

	Q_{max} (veh/min)	w (m/s)	K_{max} (veh/m)	Flow SD (veh/min)
Fixed values	40.00	-6	0.133	
Variability				
0 %	40.59	-5.95	0.136	0.49
10 %	40.87	-5.64	0.144	0.53
20 %	41.06	-5.39	0.150	0.85
30 %	41.05	-5.14	0.156	1.57

Table 3. Impact of the variability of all car-following parameters of the Newell's model on the macroscopic parameters resulting from the fitting of the fundamental diagrams of Fig. 4. The quantity "Flow SD" is the standard deviation of the flow values in the density in the range [0.035;0.040].

Car-following variability impact on macroscopic variables

Inter-vehicle variability impact on the fundamental diagram

To begin with, in Fig. 4, we present the impact of various levels of variability, with a standard deviation equals to 0 % up to 30 % of the mean values for all parameters. In this case, the U_l values are randomly selected between U_l^{min} and U_l^{max} to explore the congested branch of the FD (see state B in Fig. 1). As expected, one observes a triangular shape, consistent with Newell's model. The spreading of the congested branch increases while the variability amplitude increases. Logically, for the free flow branch, there is no evolution as we keep the same U_f without any variability thereof.

For each fundamental diagram, we fit a straight line which leads to the fitted values of the macroscopic parameters. For the case without variability (see Fig. 4-a), a small difference can be seen between the values of the fixed and fitted parameters, not greater than 3 %. This is due to the precision of the measurement method (Edie's method).

The variability amplitude has not only an impact on the spreading of the points of the congested branch, but also on

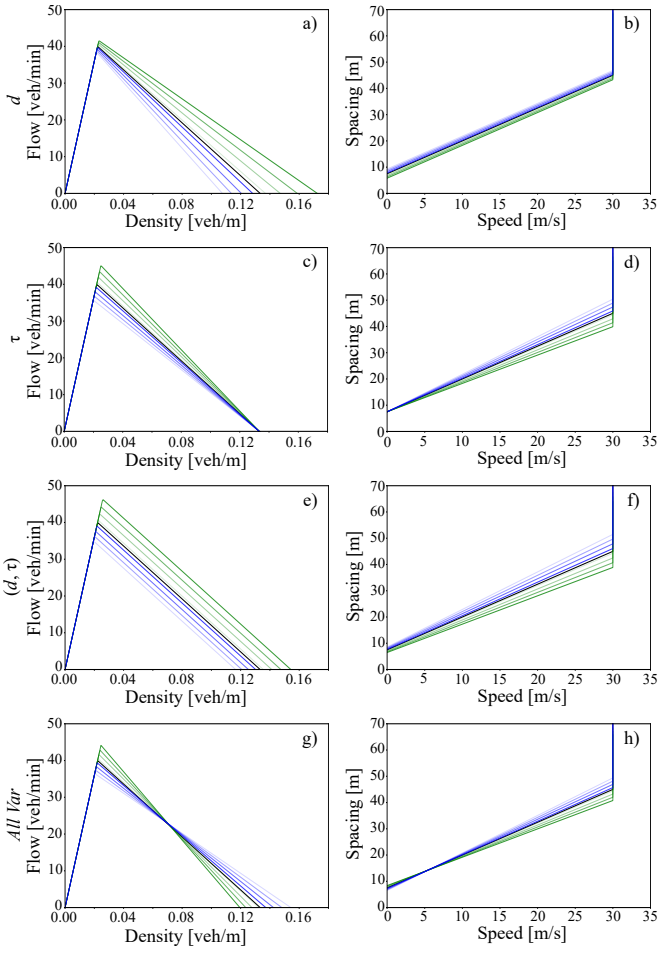

Figure 3. Parameters variation impact on the shape of the fundamental diagram (FD). Left column: macroscopic FD ($Q = f(K)$); right column: microscopic FD ($s = f'(v)$). a-b) d varies and τ remains constant, c-d) τ varies and d remains constant, e-f) the variation of τ determines the variation of d, w remaining constant, g-h) τ and d vary independently, w may vary.

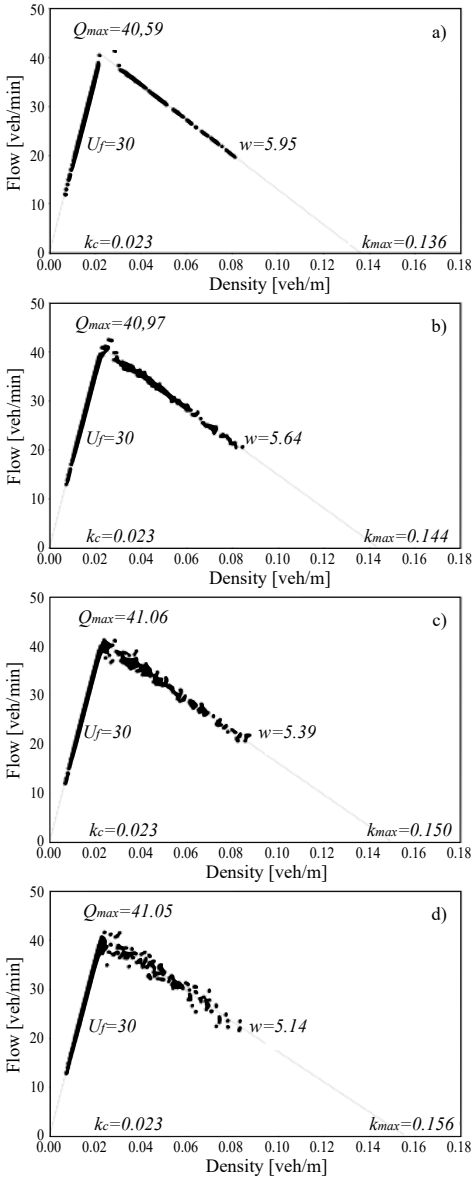

Figure 4. Fundamental diagrams obtained with different variability amplitude. The lines correspond to the best fits and the corresponding macroscopic values are presented. a) no variability, b) $\sigma_p = 0.1 \times \mu_p$, c) $\sigma_p = 0.2 \times \mu_p$, d) $\sigma_p = 0.3 \times \mu_p$, SD equals 30 % of the mean, parameters p being, reaction-time, minimal-distance and maximal-acceleration. The distribution is the truncated Gaussian. Parameters are independently varying.

the fitted macroscopic parameters values. Those observations are summarized in table 3. We evidence that w decreases 14 % and K_{max} increases 15 % as variability amplitude increases from 0 to 30 %, the Q_{max} value being almost unchanged. Keep in mind that the mean of each individual parameter remains the same. This table presents also the standard deviation of the flow in the density range from 0.03 to 0.035 veh/m, i.e. between the theoretical critical density and twice this value. This quantifies the spreading of the fundamental diagram due to the inter-vehicle variability. We can conclude that the variability amplitude has a direct impact.

Dependence of capacity on varying parameters

Fig. 5 presents the impact of each combination of parameters variability on the cumulative distribution function (cdf) of the Pre-Breakdown Capacity (PBC) and Queue Discharge Flow (QDF) for three values of speed limits. The theoretical capacity is mentioned as well as the speed limit value at the top of each column.

The table 4 synthesizes those results with the mean values of the two capacities and their standard deviations.

A global observation can be done when comparing the QDF (grey line) to the PBC (black line). The QDF mean

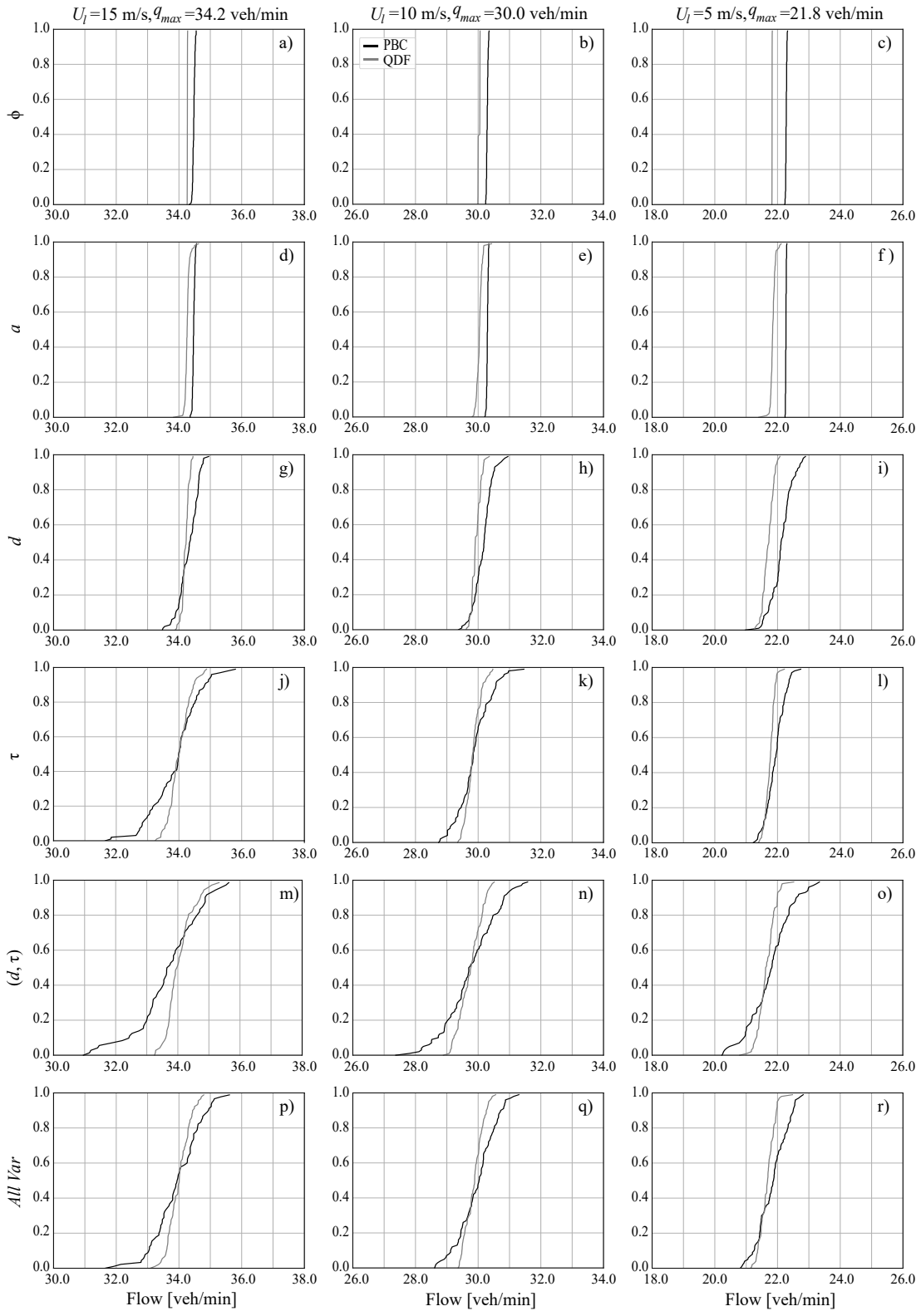

Figure 5. Impact of the CF parameters inter-vehicle variability and of the speed limit on cumulative distribution function of the PBC and QDF. The different variability configurations are organized in the rows and the three speed limits values are organized in the columns. The variability amplitude is of 20 %, the parameters are distributed according to a truncated Gaussian distribution.

Varying parameters		Speed limit 15 m/s Mean	SD	%	10 m/s Mean	SD	%	5 m/s Mean	SD	%
$\varnothing$	PBC	34,47	0,0	0,0	30,29	0,0	0,1	22,28	0,0	0,0
	QDF	34,27	0,0	0,0	30,03	0,0	0,1	21,83	0,0	0,0
a	PBC	34,47	0,0	0,1	30,30	0,0	0,1	22,27	0,0	0,1
	QDF	34,26	0,1	0,2	30,04	0,1	0,3	21,85	0,1	0,4
d	PBC	34,31	0,3	0,9	30,15	0,3	1,0	22,12	0,3	1,6
	QDF	34,21	0,1	0,3	29,94	0,1	0,5	21,70	0,2	0,8
τ	PBC	33,88	0,8	2,3	29,86	0,5	1,8	21,93	0,3	1,4
	QDF	34,01	0,3	1,0	29,84	0,2	0,8	21,76	0,3	0,7
(d, τ)	PBC	33,65	1,0	3,1	29,75	0,8	2,8	21,76	0,7	3,1
	QDF	34,04	0,4	1,3	29,74	0,4	1,3	21,65	0,3	1,3
$All\ Var$	PBC	33,93	0,8	2,2	29,96	0,6	2,0	21,84	0,5	2,2
	QDF	33,99	0,3	1,0	29,87	0,3	1,0	21,67	0,2	1,1

Table 4. Impact of the parameters variation and of the speed limit on the Pre-Breakdown Capacity (PBC) and the Queue Discharge Flow (QDF) mean values (veh/min) and standard deviations (SD).% is the ratio between SD and mean. The variability amplitude is of 20 %, the parameters are distributed according to a truncated Gaussian distribution.

value is slightly lower than the mean PBC (the difference is of the order of one percent). This is due to the fact that we adopt a version of Newell's model with a limitation in maximal acceleration. But this difference is very low and the capacity drop value we observe, compared to what is reported in the literature about CD observations, is negligible.

For the no variability case (top row), the cdfs present the typical shape of a deterministic function: no congestion occurs below the theoretical capacity, whereas in 100 % of the cases, congestion occurs for a flow value above the theoretical capacity. All the next figures are drawn with a variability amplitude of 20 % (the impact of the variability amplitude will be studied later on).

The second row of Fig. 5 presents the impact of the variability of a^n, the maximal-acceleration parameter. Its impact is negligible on the variability both of PBC and QDF, whatever the speed limit value (U_l).

Next, we vary the two other parameters: d^n and τ^n. We chose first two variability configurations where w is modified accordingly to the parameter variation, the other parameter (τ^n if we study the impact of d^n variability, d^n when τ^n varies) remaining constant.

The impact of the variability of the minimal-distance, d^n (third row), is larger than the one of the maximal-acceleration a^n. Table 4 confirms that the impact of the minimal-distance variability increases when the speed limit value decreases. Indeed, the variation of d^n has logically a bigger impact for congestion with high-density values than for light congestion.

The individual parameters variability that has the larger impact is the reaction-time τ^n. We can see on table 4 that for speed limit value of 15 m/s, the PBC variability ratio (standard deviation divided by the mean value) is of 2.3 %. Note that the variability ratio for the QDF is less than twice lower (1.0 %). Conversely to what was observed for d^n variability, τ^n variability has the larger impact when the speed limit is larger (see Fig. 5.j to 5.l).

The before the last row of this figure presents the (d, τ) case where w is constant, the individual value of d^n for a vehicle being directly determined by the one of τ^n by the relationship $d^n = w \times \tau^n$ (the variability amplitude of 20 % being applied to τ^n). We can see in this row (Fig. 5.m to .o) that the variability of the PBC and the QDF is higher in this case than in the case where τ^n varies while d^n remains constant (compare with Fig. 5.j to .l). One observes that when all parameters vary independently (Fig. 5.p to .r) the impact on the variability of the PBC is not amplified.

From what precedes, we conclude that when only one parameter is varying, the most impacting parameter, in terms of its variability, on the capacities distributions (both for the PBC and for QDF) is the reaction-time, the minimal-distance variability having a lower impact, and the maximal-acceleration distribution having a lesser impact. The relative impact of τ^n variability is larger when the speed limit is larger, the reverse effect is observed for the minimal-distance variability. When τ^n and d^n vary simultaneously, w remaining constant, the impact is maximal. This could be expected as we observe the highest spreading on the third row of Fig. 3, corresponding to this case. Combining the variability of all parameters does not significantly increases the widths of the capacities distributions.

Therefore, we consider that in our specific study case, where no lane change is possible, the maximal-acceleration variability has a very limited impact. This result must be compared with the one presented in (28) where the acceleration variability of the lane changer at merges is, by analytical calculation, proven to have a strong impact on the capacity drop. More generally, we establish that the experimental observations of the capacity drop amplitude are not linked to the distribution of the car-following parameters.

We prove, on the contrary, that CF parameters variability, *per se* has a strong impact on capacities distributions, especially when τ^n and d^n vary simultaneously, w remaining constant ((d, τ) case.).

We will now examine the impact of the distribution shapes and amplitudes in two cases, when τ^n and d^n vary simultaneously, with w constant, and when all parameters vary independently. Note that the shapes and amplitude of the distributions are, in the (d, τ) case, applied to the τ^n parameter.

Dependence of capacity variability on the distributions shapes and amplitudes

The Fig. 6 presents in two cases the cdf of PBC and of QDF for the three distributions shapes: truncated Gaussian, Gamma and Uniform, with a speed limit of $U_l = 10m/s$. The table 5 presents the corresponding numerical values for the mean and the standard deviation. Although the shapes are significantly different (as can be seen from Fig. 3), the impact on the variability amplitude of the two capacities distributions seems negligible.

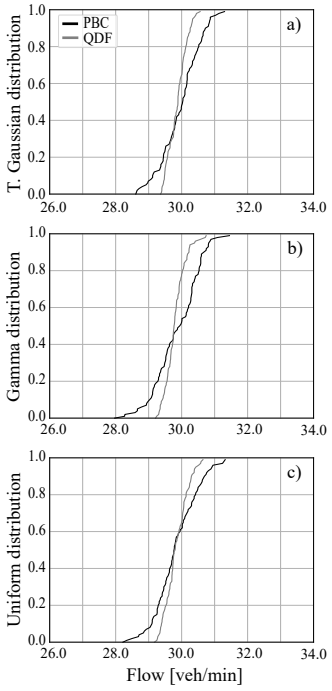

Figure 6. Impact of the shape of the distribution of the individual parameters on the capacities cumulative distribution functions. Variability amplitude if of 20 % and all the parameters vary. The speed is limited to 10 m/s.

The Fig. 7, as well as table 6, present the results for the truncated Gaussian distribution for three amplitudes: 10 %, 20 %, 30 %, with a speed limit of $U_l = 10m/s$. There is clearly a direct impact of the parameters' variability amplitude on the capacities values and on their variability amplitude. First, the mean value of the PBC decreases as the variability amplifies (from 30.29 veh/min for the no variability case, down to 29.49 veh/min for a variability amplitude of 30 %, the decrease being of 2.6 %). The same phenomenon, with a lesser impact, is observed for the QDF (from 30.03 to 29.53 veh/min, with a decrease of 1.6 %). Second, the larger the parameters amplitude the larger the capacities standard deviation. This result is coherent with what was expected.

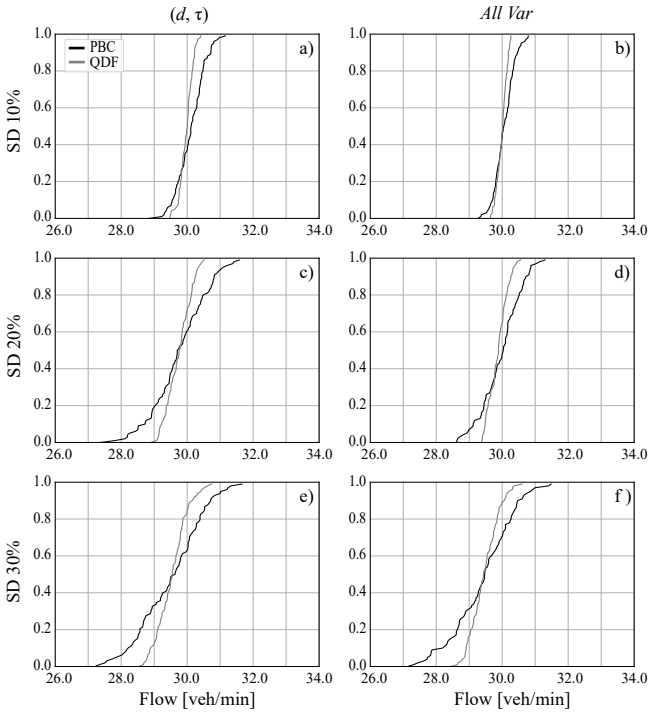

Figure 7. Impact of variability amplitude on the capacities cumulative distribution functions. The left column presents the case when τ^n and d^n vary simultaneously with constant w, the right column the case when all parameters vary independently. The three variability levels are organized in the rows. The speed is limited to 10 m/s.

Discussion and conclusions

The extensive literature review provided in this paper confirms that researchers are giving diverse and contradictory explanations for capacity distribution, capacity drop, and stop and go waves. Most of the studies in the literature address the macroscopic observations of the capacity drop and only few studies devoted to stop and go waves and capacities distribution. When trying to link the phenomena to the microscopic behaviors of vehicles, some authors argue that lane changing is the main cause of capacity drop and stop and go waves -either the inserting or the exiting events-, others consider that the random noise in acceleration is the key explanation for the capacity drop or for the stop and go waves.

		Distribution shape								
		T. Gaussian			Gamma			Uniform		
		Mean	SD	%	Mean	SD	%	Mean	SD	%
All Var	PBC	29,96	0,6	2,0	29,86	0,7	2,3	29,82	0,6	2,1
	QDF	29,87	0,3	1,0	29,80	0,3	1,0	29,83	0,3	1,1

Table 5. Impact of the shape of the distribution of the individual parameters on the capacities mean, standard deviations (SD) and on the ratio of SD over mean (%). Variability amplitude if of 20 % and all the parameters vary. The speed is limited to 10 m/s.

		(d, τ)			*All Var*		
		Mean	SD	%	Mean	SD	%
0 %	PBC	30,29	0,0	0,1	30,29	0,0	0,1
	QDF	30,03	0,0	0,1	30,03	0,0	0,1
10 %	PBC	30,11	0,4	1,4	30,06	0,3	1,0
	QDF	29,97	0,2	0,7	29,99	0,2	0,5
20 %	PBC	29,75	0,8	2,8	29,96	0,6	2,0
	QDF	29,74	0,4	1,3	29,87	0,3	1,0
30 %	PBC	29,49	1,0	3,3	29,40	0,9	3,2
	QDF	29,53	0,5	1,6	29,45	0,4	1,5

Table 6. Impact of variability amplitude on the capacities mean, standard deviations (SD) and on the ratio of SD over mean (%). The central columns present the case when τ^n and d^n vary simultaneously with constant w, the right columns the case when all parameters vary independently. The three variability levels are organized in the rows. The speed is limited to 10 m/s.

In the current work, we quantify the impact of the individual parameters variability of the car-following part of the microscopic behavior of the vehicles. We choose this approach not because we neglect the impact of lane change. We believe the two aspects need first to be addressed separately. The combination of lane change behaviors and car following distribution is left for future research.

We define a simple simulation test-bed to create a bottleneck by considering only car-following behavior. A speed limit has been imposed in a part of the one-lane stretch of road. We use the classical Newell's model (*18*), expressed after (*19*) in terms of speed, chosen for its ease of interpretation and for its simplicity. We focused here on the following three parameters characterizing the individual behavior of the driver-vehicle pairs: minimal-distance d^n, reaction-time τ^n and maximal-acceleration a^n.

We did not observe any impact of the car-following parameters on the capacity drop: the difference between the Pre-Breakdown Capacity and the Queue Discharge Flow is lower than 1 % in all the studied configurations. Note that we did chose a rather large mean value of the maximal-acceleration of 2.5 m/s^2.

Our results show that among those three parameters, the reaction-time variability has the larger impact on the capacities distribution. This can be explained by the figure 3, where we can see, on the second row, that the capacity variability is higher than in the first row where d varies. Moreover, an uncertainty propagation calculus can confirm this. The flow associated to a congested regime whose speed is limited to u is expressed, with the Newell's model as:

$$C_u = \frac{1}{(\tau + d/u)} \tag{2}$$

Applying the uncertainty propagation method in the case of independence of parameters d and τ, one obtains the value of the relative variation of C_u:

$$\frac{\sigma^2_{C_u}}{{C_u}^2} = \frac{\sigma^2_\tau + \sigma^2_d/u^2}{(\tau + d/u)^2} \tag{3}$$

Since the variance σ^2_d for the parameter d is divided by the square of the speed limit u, the weight of this variance in the relative variance of the capacity is less than that of the parameter τ.

The impact is higher when all the three parameters vary, the maximal-acceleration a independently, and the minimal-distance parameter d, in conjunction with reaction-time τ, permitting to keep w, the backward wave propagation speed, constant. The maximal impact was obtained in the case where the variability amplitude of each parameter is of 30 %, which corresponds to the highest studied amplitude. We did not observe a significant impact of the distribution function on any macroscopic characteristic (capacity drop or capacities variability). We compared the most classical distributions: Gamma, truncated Gaussian, and uniform.

Compared to the capacity distribution observations reported in the literature, our results explain between an $1/2$ and a $1/3$ of the standard deviations (mean std of 7.2 % for (*3*) and of 9.4 % for (*11*)). This means that the car following parameters contribution to the capacity distribution is far from being negligible. We realize exactly the same study with the Gipps' car following model and obtained similar results (*53*).

The key finding in this work is the significant impact of the distribution of the reaction-time τ^n parameter. In many microscopic simulation tools, τ^n is equal to the computation time-step and therefore uniform for all vehicles. From our results we can clearly conclude that any simulation study willing to scrutinize the variability among days concerning congestion creation, duration and amplitude, ignoring the variability of the reaction time will fail to reach its goals.

Moreover, microscopic simulation tools are often used to test traffic control methods. The simplification brought by the

using of a unique value for the reaction time is a potential source of erroneous estimation of the impact of these controls on the basis of microscopic simulation tools.

Future researches will be devoted to the study of lane changes impacts on the capacity drop and the capacity distribution, with a focus on the behavior variability among driver-vehicles pairs.

Authors' contributions statement

C.M.G.P., C.B. and M.K.E. designed the study. C.M.G.P. performed the simulation experiments. All authors contributed to the interpretation of the results. C.B. and C.M.G.P. took the lead in writing the manuscript. All authors provided critical feedback and contributed to the final version of the manuscript.

References

1. Chung, K., J. Rudjanakanoknad, and M. J. Cassidy. Relation between traffic density and capacity drop at three freeway bottlenecks. *Transportation Research Part B: Methodological*, Vol. 41, No. 1, 2007, pp. 82–95. doi:10.1016/j.trb.2006.02.011. URL http://www.sciencedirect.com/science/article/pii/S0191261506000397.
2. Oh, S. and H. Yeo. Estimation of Capacity Drop in Highway Merging Sections. *Transportation Research Record*, Vol. 2286, No. 1, 2012, pp. 111–121. doi:10.3141/2286-13. URL http://journals.sagepub.com/doi/10.3141/2286-13.
3. Kondyli Alexandra, George Bryan St., Elefteriadou Lily, and Bonyani Gina. Defining, Measuring, and Modeling Capacity for the Highway Capacity Manual. *Journal of Transportation Engineering, Part A: Systems*, Vol. 143, No. 3, 2017, p. 04016014. doi:10.1061/JTEPBS.0000017. URL https://ascelibrary.org/doi/full/10.1061/JTEPBS.0000017.
4. Cassidy, M. J. and J. Rudjanakanoknad. Increasing the capacity of an isolated merge by metering its on-ramp. *Transportation Research Part B: Methodological*, Vol. 39, No. 10, 2005, pp. 896–913. doi:10.1016/j.trb.2004.12.001. URL http://www.sciencedirect.com/science/article/pii/S0191261505000044.
5. Srivastava, A. and N. Geroliminis. Empirical observations of capacity drop in freeway merges with ramp control and integration in a first-order model. *Transportation Research Part C: Emerging Technologies*, Vol. 30, 2013, pp. 161–177. doi:10.1016/j.trc.2013.02.006. URL http://www.sciencedirect.com/science/article/pii/S0968090X13000363.
6. Cho, H. W. and J. A. Laval. Combined Ramp-Metering and Variable Speed Limit System for Capacity Drop Control at Merge Bottlenecks. *Journal of Transportation Engineering, Part A: Systems*, Vol. 146, No. 6, 2020, p. 04020033. doi:10.1061/JTEPBS.0000350. URL https://ascelibrary.org/doi/abs/10.1061/JTEPBS.0000350. Publisher: American Society of Civil Engineers.
7. Zhu, H. B., Y. J. Zhou, and W. J. Wu. Modeling traffic flow mixed with automated vehicles considering drivers ' character difference. *Physica A: Statistical Mechanics and its Applications*, Vol. 549, 2020, p. 124337. doi:10.1016/j.physa.2020.124337. URL http://www.sciencedirect.com/science/article/pii/S0378437120301138.
8. Ibrahim, A. T. and F. L. Hall. Effect of adverse weather conditions on speed-flow-occupancy relationship. *Transportation Research Record*, , No. 1457. URL https://trid.trb.org/view/425358.
9. Hall, F. L. and K. Agyemang-Duah. Freeway capacity drop and the definition of capacity. *Transportation Research Record*, , No. 1320. URL https://trid.trb.org/view/365591.
10. Lorenz, M. and L. Elefteriadou. A Probabilistic Approach to Defining Freeway Capacity and Breakdown. In *Transportation Research Circular E-CO18, (4th International Symposium on Highway Capacity) Transportation Research Board, National Research Council*. 2000, pp. 84–85.
11. Brilon, W., J. Geistefeldt, and M. Regler. Reliability of Freeway Traffic Flow. In *Transportation and Traffic Theory*. Elsevier, 2005, pp. 125–144. doi:10.1016/B978-008044680-6/50009-X. URL https://linkinghub.elsevier.com/retrieve/pii/B978008044680650009X.
12. Xie, K., K. Ozbay, D. Yang, H. Yang, and Y. Zhu. Modeling lane-specific breakdown probabilities at freeway diverge sections. *Physica A: Statistical Mechanics and its Applications*, Vol. 561, 2021, p. 125231. doi:10.1016/j.physa.2020.125231. URL http://www.sciencedirect.com/science/article/pii/S037843712030649X.
13. Yuan, K., V. L. Knoop, and S. P. Hoogendoorn. Capacity drop: a relation between the speed in congestion and the queue discharge rate. *Transportation Research Record: Journal of the Transportation Research Board*, Vol. 2491, 2015, pp. 72–80. doi:10.3141/2491-08. URL https://trrjournalonline.trb.org/doi/abs/10.3141/2491-08.
14. Yuan, K., V. L. Knoop, L. Leclercq, and S. P. Hoogendoorn. Capacity drop: a comparison between stop-and-go wave and standing queue at lane-drop bottleneck. *Transportmetrica B: Transport Dynamics*, Vol. 5, No. 2, 2017, pp. 145–158. doi:10.1080/21680566.2016.1245163. URL https://doi.org/10.1080/21680566.2016.1245163. Publisher: Taylor & Francis _eprint: https://doi.org/10.1080/21680566.2016.1245163.
15. Chen, D., S. Ahn, J. Laval, and Z. Zheng. On the periodicity of traffic oscillations and capacity drop: The role of driver characteristics. *Transportation Research Part B: Methodological*, Vol. 59, 2014, pp. 117–136. doi:10.1016/j.trb.2013.11.005. URL http://www.sciencedirect.com/science/article/pii/S0191261513002117.

16. Oh, S. and H. Yeo. Impact of stop-and-go waves and lane changes on discharge rate in recovery flow. *Transportation Research Part B: Methodological*, Vol. 77, 2015, pp. 88–102. doi:10.1016/j.trb.2015.03.017. URL http://www.sciencedirect.com/science/article/pii/S0191261515000600.
17. Calvert, S. C., H. Taale, M. Snelder, and S. P. Hoogendoorn. Application of advanced sampling for efficient probabilistic traffic modelling. Vol. 49, , pp. 87–102. doi:10.1016/j.trc.2014.10.013. URL https://www.sciencedirect.com/science/article/pii/S0968090X14003131.
18. Newell, G. F. A simplified car-following theory: a lower order model. *Transportation Research Part B: Methodological*, Vol. 36, No. 3, 2002, pp. 195–205. doi:10.1016/S0191-2615(00)00044-8. URL http://www.sciencedirect.com/science/article/pii/S0191261500000448.
19. Jabari, S. E., J. Zheng, and H. X. Liu. A probabilistic stationary speed–density relation based on Newell's simplified car-following model. *Transportation Research Part B: Methodological*, Vol. 68, 2014, pp. 205–223. doi:10.1016/j.trb.2014.06.006. URL http://www.sciencedirect.com/science/article/pii/S0191261514001131.
20. Leclercq, L., N. Chiabaut, J. Laval, and C. Buisson. Relaxation Phenomenon After Lane Changing: Experimental Validation with NGSIM Data Set. *Transportation Research Record: Journal of the Transportation Research Board*, Vol. 1999, 2007, pp. 79–85. doi:10.3141/1999-09. URL https://trrjournalonline.trb.org/doi/abs/10.3141/1999-09.
21. Laval, J. A. and L. Leclercq. Microscopic modeling of the relaxation phenomenon using a macroscopic lane-changing model. *Transportation Research Part B: Methodological*, Vol. 42, No. 6, 2008, pp. 511–522. doi:10.1016/j.trb.2007.10.004. URL http://www.sciencedirect.com/science/article/pii/S0191261507001312.
22. Duret, A., J. Bouffier, and C. Buisson. Onset of Congestion from Low-Speed Merging Maneuvers within Free-Flow Traffic Stream: Analytical Solution. *Transportation Research Record*, Vol. 2188, No. 1, 2010, pp. 96–107. doi:10.3141/2188-11. URL https://doi.org/10.3141/2188-11.
23. Kim, S. and B. Coifman. Driver relaxation impacts on bottleneck activation, capacity, and the fundamental relationship. *Transportation Research Part C: Emerging Technologies*, Vol. 36, 2013, pp. 564–580. doi:10.1016/j.trc.2013.06.016. URL http://www.sciencedirect.com/science/article/pii/S0968090X13001393.
24. Zheng, Z., S. Ahn, D. Chen, and J. Laval. The effects of lane-changing on the immediate follower: Anticipation, relaxation, and change in driver characteristics. *Transportation Research Part C: Emerging Technologies*, Vol. 26, 2013, pp. 367–379. doi:10.1016/j.trc.2012.10.007. URL http://www.sciencedirect.com/science/article/pii/S0968090X12001295.
25. Ahn, S. and M. J. Cassidy. Freeway Traffic Oscillations and Vehicle Lane-Change Maneuvers. 2007. URL https://trid.trb.org/view/820158.
26. Mauch, M. and M. J. Cassidy. Freeway traffic oscillations: observations and predictions. URL https://escholarship.org/uc/item/89c3h1vv.
27. Zheng, Z., S. Ahn, D. Chen, and J. Laval. Freeway Traffic Oscillations: Microscopic Analysis of Formations and Propagations using Wavelet Transform. *Procedia - Social and Behavioral Sciences*, Vol. 17, 2011, pp. 702–716. doi:10.1016/j.sbspro.2011.04.540. URL https://linkinghub.elsevier.com/retrieve/pii/S1877042811010998.
28. Leclercq, L., V. L. Knoop, F. Marczak, and S. P. Hoogendoorn. Capacity drops at merges: New analytical investigations. *Transportation Research Part C: Emerging Technologies*, Vol. 62, 2016, pp. 171–181. doi:10.1016/j.trc.2015.06.025. URL http://www.sciencedirect.com/science/article/pii/S0968090X15002405.
29. Coifman, B. and S. Kim. Extended Bottlenecks, the Fundamental Relationship, and Capacity Drop on Freeways. *Procedia - Social and Behavioral Sciences*, Vol. 17, 2011, pp. 44–57. doi:10.1016/j.sbspro.2011.04.507. URL http://www.sciencedirect.com/science/article/pii/S1877042811010664.
30. Leclercq, L., J. A. Laval, and N. Chiabaut. Capacity Drops at Merges: an endogenous model. *Procedia - Social and Behavioral Sciences*, Vol. 17, 2011, pp. 12–26. doi:10.1016/j.sbspro.2011.04.505. URL http://www.sciencedirect.com/science/article/pii/S1877042811010640.
31. Han, Y. and S. Ahn. Stochastic modeling of breakdown at freeway merge bottleneck and traffic control method using connected automated vehicle. *Transportation Research Part B: Methodological*, Vol. 107, 2018, pp. 146–166. doi:10.1016/j.trb.2017.11.007. URL http://www.sciencedirect.com/science/article/pii/S0191261517302990.
32. Yang, Y., K. Wada, T. Oguchi, and M. Iryo-Asano. Variability of observed drivers' car-following behavior on expressway basic segment. *Transportation Research Procedia*, Vol. 25, 2017, pp. 1503–1532. doi:10.1016/j.trpro.2017.05.179. URL http://www.sciencedirect.com/science/article/pii/S2352146517304726.
33. Wong, G. C. K. and S. C. Wong. A multi-class traffic flow model – an extension of LWR model with heterogeneous drivers. *Transportation Research Part A: Policy and Practice*, Vol. 36, No. 9, 2002, pp. 827–841. doi:10.1016/S0965-8564(01)00042-8. URL http://www.sciencedirect.com/science/article/pii/S0965856401000428.
34. Ossen, S. and S. P. Hoogendoorn. Driver Heterogeneity in Car following and Its Impact on Modeling Traffic Dynamics. *Transportation Research Record*, Vol. 1999, No. 1, 2007, pp. 95–103. doi:10.3141/1999-11. URL http://journals.sagepub.com/doi/10.3141/1999-11.

35. Laval Jorge A. and Leclercq Ludovic. A mechanism to describe the formation and propagation of stop-and-go waves in congested freeway traffic. *Philosophical Transactions of the Royal Society A: Mathematical, Physical and Engineering Sciences*, Vol. 368, No. 1928, 2010, pp. 4519–4541. doi:10.1098/rsta.2010.0138. URL https://royalsocietypublishing.org/doi/full/10.1098/rsta.2010.0138.
36. Calvert, S. C., F. L. M. van Wageningen-Kessels, and S. P. Hoogendoorn. Capacity drop through reaction times in heterogeneous traffic. *Journal of Traffic and Transportation Engineering*, Vol. 5, No. 2, 2018, pp. 96–104. doi:10.1016/j.jtte.2017.07.008. URL http://www.sciencedirect.com/science/article/pii/S2095756417300041.
37. Zhang, H. M. and T. Kim. A car-following theory for multiphase vehicular traffic flow. *Transportation Research Part B: Methodological*, Vol. 39, No. 5, 2005, pp. 385–399. doi:10.1016/j.trb.2004.06.005. URL http://www.sciencedirect.com/science/article/pii/S0191261504000864.
38. Yuan, K., J. Laval, V. L. Knoop, R. Jiang, and S. P. Hoogendoorn. A geometric Brownian motion car-following model: towards a better understanding of capacity drop. *Transportmetrica B: Transport Dynamics*, Vol. 7, No. 1, 2019, pp. 915–927. doi:10.1080/21680566.2018.1518169. URL https://www.tandfonline.com/doi/10.1080/21680566.2018.1518169.
39. Xu, T. and J. A. Laval. Analysis of a two-regime stochastic car-following model: explaining capacity drop and oscillation instabilities. *Transportation Research Record*, 2019, pp. 610–619. URL https://doi.org/10.1177/0361198119850464.
40. Xu, T. and J. Laval. Statistical inference for two-regime stochastic car-following models. *Transportation Research Part B: Methodological*, Vol. 134, 2020, pp. 210–228. doi:10.1016/j.trb.2020.02.003. URL http://www.sciencedirect.com/science/article/pii/S019126151830955X.
41. Treiber, M. and A. Kesting. The Intelligent Driver Model with Stochasticity -New Insights Into Traffic Flow Oscillations. *Transportation Research Procedia*, Vol. 23, 2017, pp. 174–187. doi:10.1016/j.trpro.2017.05.011. URL http://www.sciencedirect.com/science/article/pii/S2352146517302880.
42. Ngoduy, D., S. Lee, M. Treiber, M. Keyvan-Ekbatani, and H. L. Vu. Langevin method for a continuous stochastic car-following model and its stability conditions. *Transportation Research Part C: Emerging Technologies*, Vol. 105, 2019, pp. 599–610. doi:10.1016/j.trc.2019.06.005. URL http://www.sciencedirect.com/science/article/pii/S0968090X1831773X.
43. Laval, J. A., C. S. Toth, and Y. Zhou. A parsimonious model for the formation of oscillations in car-following models. *Transportation Research Part B: Methodological*, Vol. 70, 2014, pp. 228–238. doi:10.1016/j.trb.2014.09.004. URL http://www.sciencedirect.com/science/article/pii/S0191261514001581.
44. Treiber, M., A. Kesting, and D. Helbing. Influence of Reaction Times and Anticipation on Stability of Vehicular Traffic Flow. *Transportation Research Record*, Vol. 1999, No. 1, 2007, pp. 23–29. doi:10.3141/1999-03. URL http://journals.sagepub.com/doi/10.3141/1999-03.
45. Goni Ros, B., V. L. Knoop, B. van Arem, and S. Hoogendoorn. Car-following behavior at sags and its impacts on traffic flow. 2013. URL https://trid.trb.org/view/1241235.
46. Corman, F., A. Trivella, and M. Keyvan-Ekbatani. Stochastic process in railway traffic flow: Models, methods and implications. *Transportation Research Part C: Emerging Technologies*, Vol. 128, 2021, p. 103167. doi:https://doi.org/10.1016/j.trc.2021.103167. URL https://www.sciencedirect.com/science/article/pii/S0968090X21001856.
47. Kaur, R. and S. Sharma. Modeling and simulation of driver's anticipation effect in a two lane system on curved road with slope. *Physica A: Statistical Mechanics and its Applications*, Vol. 499, 2018, pp. 110–120. doi:10.1016/j.physa.2017.12.101. URL http://www.sciencedirect.com/science/article/pii/S0378437117313511.
48. Chen, D. and S. Ahn. Capacity-drop at extended bottlenecks: Merge, diverge, and weave. *Transportation Research Part B: Methodological*, Vol. 108, 2018, pp. 1–20. doi:10.1016/j.trb.2017.12.006. URL http://www.sciencedirect.com/science/article/pii/S0191261517306938.
49. Chen, D., J. Laval, Z. Zheng, and S. Ahn. A behavioral car-following model that captures traffic oscillations. *Transportation Research Part B: Methodological*, Vol. 46, No. 6, 2012, pp. 744–761. doi:10.1016/j.trb.2012.01.009. URL http://www.sciencedirect.com/science/article/pii/S0191261512000136.
50. Ossen, S. and S. P. Hoogendoorn. Heterogeneity in car-following behavior: Theory and empirics. *Transportation Research Part C: Emerging Technologies*, Vol. 19, No. 2, 2011, pp. 182–195. doi:10.1016/j.trc.2010.05.006. URL http://www.sciencedirect.com/science/article/pii/S0968090X10000902.
51. Edie, L. C. Discussion of traffic stream measurements and definitions. *Proceedings of the Second International Symposium on the Theory of Traffic Flow, London 1963.*, 1965, pp. 139–154.
52. Chiabaut, N., L. Leclercq, and C. Buisson. From heterogeneous drivers to macroscopic patterns in congestion. *Transportation Research Part B: Methodological*, Vol. 44, No. 2, 2010, pp. 299–308. doi:10.1016/j.trb.2009.07.009. URL http://www.sciencedirect.com/science/article/pii/S0191261509000976.
53. Gomez-Patiño, C. M. Variabilité inter-individuelle du comportement longitudinal de véhicules à conduite manuelle ou automatisée : impacts sur la capacité des voies.